

See discussions, stats, and author profiles for this publication at: <https://www.researchgate.net/publication/51237738>

Thermal Rate Constant Calculation of the NF + F Reactive System Multiple Arrangements

ARTICLE in THE JOURNAL OF PHYSICAL CHEMISTRY A · JUNE 2011

Impact Factor: 2.69 · DOI: 10.1021/jp204229d · Source: PubMed

CITATION

1

READS

30

7 AUTHORS, INCLUDING:



Patricia Barreto

National Institute for Space Research, Brazil

49 PUBLICATIONS 270 CITATIONS

SEE PROFILE



Pedro Henrique de Oliveira Neto

University of Brasília

28 PUBLICATIONS 154 CITATIONS

SEE PROFILE



Geraldo Magela e Silva

University of Brasília

90 PUBLICATIONS 509 CITATIONS

SEE PROFILE



Ricardo Gargano

University of Brasília

102 PUBLICATIONS 601 CITATIONS

SEE PROFILE


Thermal Rate Constant Calculation of the NF + F Reactive System Multiple Arrangements

Simone S. Ramalho,[†] Wiliam F. da Cunha,[‡] Patrícia R. P. Barreto,[§] Pedro H. O. Neto,[‡] Luiz F. Roncaratti,[‡] Geraldo Magela e Silva,[‡] and Ricardo Gargano^{*,‡}

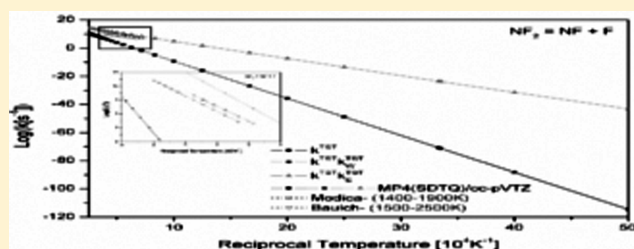
[†]Instituto Federal de Educação, Ciência e Tecnologia de Goiás Av. Universitária, Vale das Goiabeiras, Inhumas, GO, CEP 75400-000, Brazil

[‡]Instituto de Física, Universidade de Brasília, CP04455, Brasília, DF, CEP 70919-970, Brazil

[§]LAP, Instituto Nacional de Pesquisas Espaciais, CP515, São José dos Campos, SP, CEP 12247-970, Brazil

 Supporting Information

ABSTRACT: In this work we analyzed the multiple channels of the reaction $\text{NF} + \text{F}$ through the evaluation of thermal rate constants with both Wigner and Eckart tunneling corrections. Minimum energy paths and intrinsic reaction coordinates of the systems were obtained and accurately studied in order to ensure the consistency of our results. Specifically, we investigated the $\text{NF} + \text{F} = \text{N} + \text{F}_2$, $\text{NF} + \text{F} = \text{NF} + \text{F}$, and $\text{NF}_2 = \text{NF} + \text{F}$, reactive systems. As experimental data are available for the latter reaction, we were able to conclude that our thermal rate constants are in agreement for a wide range of temperatures. The here performed study is relevant to the understanding of the decomposition process of nitrogen trifluoride (NF_3).



INTRODUCTION

Nitrogen trifluoride (NF_3) was first synthesized in the late 20s. Nowadays it is an extensively used gas in the electronics industry as well as in excimer laser systems, besides other technological uses.^{1–3} As the search for cleaner substitutes in terms of emission to the environment gained importance in the last decades, it is observed a natural rise in the production of NF_3 .² Compared to other fluorinated gases, such as CF_4 and C_2F_6 , NF_3 has the advantage of avoiding the contamination with carbon residuals. Since the emission of nitrogen trifluoride became important, it is fundamental, from the environment point of view, to understand the mechanism of decomposition of this compound. In this sense, we intend to study the decomposition of NF_3 in nitrogen and fluorine species.⁴

To understand the actual dissociation path of nitrogen trifluoride, a simple kinetic mechanism composed of several elementary reactions is proposed. The idea is that these elementary reactions would take part as intermediary steps to reach the global reaction. This mechanism would contain the several associations listed as:

- Unimolecular ($\text{NF} = \text{N} + \text{F}$, $\text{NF}_2 = \text{NF} + \text{F}$, $\text{NF}_3 = \text{NF}_2 + \text{F}$, $\text{N}_2\text{F} = \text{N}_2 + \text{F}$, $\text{N}_2\text{F}_3 = \text{NF}_2 + \text{NF}$).
- Abstraction ($\text{NF}_2 + \text{F} = \text{NF} + \text{F}_2$, $\text{NF}_3 + \text{F} = \text{NF}_2 + \text{F}_2$, $\text{NF} + \text{N} = \text{N}_2 + \text{F}$, $\text{NF}_3 + \text{N} = \text{NF}_2 + \text{NF}$).
- Exchange ($\text{NF} + \text{F} = \text{NF} + \text{F}$, $\text{NF}_2 + \text{F} = \text{NF}_2 + \text{F}$, $\text{NF}_3 + \text{F} = \text{NF}_3 + \text{F}$).

Overall, there are a total of 14 reactions that make part of a gas-phase kinetic mechanisms for N/F/H system.

It is a well-known fact that Transition State Theory (TST) has been successful in calculating the standard enthalpy, entropy, and Gibbs energy of activation for a particular reaction if its rate constant has been experimentally determined. Therefore, TST consists of a very useful tool when it comes to the qualitative understanding of how chemical reactions take place.

This paper is dedicated to the study of three of the elementary reactions in the scope of the TST approach, consisting of a continuation of our previous work.⁵ We initially dealt with two channels of the reaction involving NF: $\text{NF} + \text{F} = \text{NF} + \text{F}$ (exchange) and $\text{NF} + \text{F} = \text{N} + \text{F}_2$ (abstraction). Also, the unimolecular decomposition $\text{NF}_2 = \text{NF} + \text{F}$ was investigated as we obtained a TST rate constant in excellent agreement with experimental data available in the literature. It is worthy to mention that in our development we included two different tunneling effect corrections for TST (Wigner⁶ and Eckart⁷).

This paper is organized as follows. In section 2 we present our model, where the main features of our code as well as the computational details are discussed. Our results are presented in section 3 and the conclusions are presented at section 4.

MODEL

As it will be discussed latter in this section, to apply TST we must know the geometries, frequencies, and the potential energy

Received: May 6, 2011

Revised: June 17, 2011

Published: June 21, 2011

for the reactants, products and transition state (TS) of the $\text{NF} + \text{F} = \text{N} + \text{F}_2$, $\text{NF} + \text{F} = \text{NF} + \text{F}$, and $\text{NF}_2 = \text{NF} + \text{F}$ reactions.

To obtain the mentioned quantities, we performed accurate electronic structure calculations using the Gaussian 03 program⁸ with different basis sets and levels of theory. The TS of these reactions were determined using the full (all electrons included in the correlation calculation) second order Møller-Plesset (MP2) level of theory with the 6-31G(d) and cc-pVDZ basis sets.

The desired level of accuracy for our data was reached by using extended basis sets at higher levels of theory. We determined two sets of energies for these reactions. Starting from MP2/cc-pVDZ optimized geometries, the first set was determined using the aug-cc-pVDZ, cc-pVTZ and aug-cc-pVTZ Dunning basis sets at MP4-(SDQ), MP4(SDTQ), QCISD, QCISD(T), CCSD, and CCSD(T) levels. The second set was determined starting from MP2/6-31G(d) optimized geometries at the same six levels of calculations and the following Pople basis sets: 6-31++G(d,p), 6-311++G(d,p), 6-311++G(df,pd), and 6-311++G(3df,3pd). The frequencies related to each reaction were scaled by the factors 0.977884 and 0.962846 for the cc-pVDZ and 6-31G(d) basis sets, respectively. The scale factor was calculated in the same fashion as in ref 5.

In the scope of the transition state theory, the energies, frequencies, and geometries obtained through these methods are used to calculate the partition functions of reactants, transition state, and products.⁹

By using TST, the thermal rate constant (TRC) of a general bimolecular reaction such as $\text{A} + \text{BC} \rightarrow \text{X}^\ddagger \rightarrow \text{C} + \text{AB}$ can be written as^{6,9–12}

$$k^{\text{TST}} = \frac{k_{\text{B}}T}{h} \frac{Q_{\text{X}^\ddagger}}{Q_{\text{A}}Q_{\text{BC}}} \exp\left(-\frac{V_a^{\text{G}}}{RT}\right) \quad (1)$$

where Q_{X^\ddagger} , Q_{A} , and Q_{BC} are the partition functions of TS and reactants ($\text{A} + \text{BC}$), respectively. k_{B} is the Boltzmann's constant, h is the Planck's constant, T is the temperature, R is the universal gas constant, and V_a^{G} is the potential barrier:

$$V_a^{\text{G}} = V_{\text{MEP}} + \varepsilon_{\text{ZPE}} \quad (2)$$

where ε_{ZPE} is the harmonic zero-point energies (ZPE) and V_{MEP} (minimum energy path) is the Eckart classical potential energy point⁷ measured from the overall zero energy of the reactants:

$$V_{\text{MEP}} = \frac{ay}{1+y} + \frac{by}{(1+y)^2} \quad (3)$$

where

$$y = e^{\alpha(s-s_0)} \quad (4)$$

$$a = \Delta H_0^0 = V_a^{\text{G}^\ddagger}(s = +\text{inf}) - V_a^{\text{G}^\ddagger}(s = -\text{inf}) \quad (5)$$

$$b = (2V_a^{\text{G}^\ddagger} - a) + 2(V_a^{\text{G}^\ddagger}(V_a^{\text{G}^\ddagger} - a))^{1/2} \quad (6)$$

$$s_0 = -\frac{1}{\alpha} \ln\left(\frac{a+b}{b-a}\right) \quad (7)$$

$$\alpha^2 = -\frac{\mu(\omega^\ddagger)^2 b}{2V_a^{\text{G}^\ddagger}(V_a^{\text{G}^\ddagger} - a)} \quad (8)$$

Here μ is the reduced mass, a and b depend on the reactants ($V_a^{\text{G}^\ddagger}(s = -\text{inf})$), products ($V_a^{\text{G}^\ddagger}(s = +\text{inf})$), and TS ($V_a^{\text{G}^\ddagger}$) energies, as

Table 1. Geometry parameters for reactants and products F_2 , NF , and NF_2 calculated through MP2/cc-pVDZ e 6-31G(d) (interatomic distances given in Å and bond angles in degrees)

species	basis	interatomic distances		bond angles
		R_{NF}	R_{FF}	A_{FNF}
F_2	cc-pVDZ		1.424	
	6-31G(d)		1.421	
	exp. ref.		1.4119 ¹⁹	
			1.412 ²⁰	
			1.435 ²¹	
NF			1.421 ²²	
	theor. ref.			
	cc-pVDZ	1.317		
	6-31G(d)	1.330		
	Exp. ref.	1.3173 ²³		
NF_2				
	cc-pVDZ	1.349		103.658
	6-31G(d)	1.359		103.262
	exp. ref.	1.370 ^{24,25}		104.2 ^{24,25}
	theor. ref.	1.359		103.3

well as the imaginary frequency on the TS (ω^\ddagger).^{13,14} y is a parameter related to the reaction coordinate.

To take into account tunneling effects along the reaction coordinate, we introduce the transmission coefficient $\kappa_{\text{W/E}}(T)$ ^{15,16} in the conventional TST, as follows

$$k = \kappa_{\text{W/E}}(T)k^{\text{TST}}(T) \quad (9)$$

where $\kappa_{\text{W/E}}(T)$ stands for Wigner or Eckart correction. The coefficients for these tunneling corrections are detailed presented in ref 5. It is worthy to mention that, because of the parabolic potential considered in the Wigner correction, the TRC thus obtained is known to yield underestimated values in relation to the Eckart correction.

The characteristics of the MEP and the TRC, with the Wigner and Eckart tunneling corrections, were determined using our own code, which is described in the literature.^{10–12} The TRC were then expressed in the Arrhenius form as

$$k(T) = AT^N \exp\left(-\frac{E_a}{RT}\right) \quad (10)$$

where A is the pre-exponential factor, N is the temperature power factor, and E_a is the activation energy.

RESULTS AND DISCUSSION

We start this section comparing geometry, frequency, and energy results of the different reactions and then devote the remaining of the section to the rate constant study.

Table 1 presents the equilibrium geometries for all species of our systems, calculated at the full MP2 level with cc-pVDZ, 6-31g, and aug-cc-pVTZ basis. Also, experimental and theoretical data are available for comparison purposes. It is clear the good agreement that both our distances and our angle values present when compared with other works in the literature. The largest absolute error in distance was of 0.014 for F_2 , 0.19 for NF and 0.02 for NF_2 . As for the angle, we obtained a maximum absolute

Table 2. Harmonic Vibrational Frequencies (cm^{-1}) and Zero-Point Energy (kcal/mol) for F_2 , NF , and NF_2 Calculated through MP2/cc-pVDZ and 6-31G(d)

species	basis	ν_1	ν_2	ν_3	ϵ_{ZPE}
F_2	cc-pVDZ	933.42			1.305
	6-31G(d)	1007.75			1.387
	exp. ref.	892.0 ^{21,26}			
NF		916.4 ²⁰			
	theor. ref.	2118.7			
	cc-pVDZ	1175.3			1.643
	6-31G(d)	1192.0			1.641
	exp. ref.	1115.0 ¹⁹			
NF_2		1141.4 ^{20,23}			
	theor. ref.	1138.5 ²³			
		1104.6 ²²			
	cc-pVDZ	585.97	982.77	1126.61	
	6-31G(d)	573.89	1026.08	1147.01	3.768
	exp. ref.	573 ¹⁹	931 ¹⁹	1047 ¹⁹	3.781
	exp. ref.	573.4 ²⁵	930.7 ²⁵	1069.5 ²⁵	

error of 0.938° for the latter structure. All these error values are small enough to be neglected as far as their inclusion in the TST formalism is concerned.

Following, we calculated the frequencies for the three molecular species involved in the reactions. To take into account the deficiencies of the MP2 level for the used basis set, the frequencies were properly scaled as described in ref 5. Our simulations again yielded values with little average errors when compared with experimental results. As can be seen in Table 2, the vibrational frequencies systematically presented values slightly larger than those of experimental data. This fact can be attributed to peculiarities in the experiments, such as concentration of catalysts, features not covered by our model.

Another important correction also performed in this work is the so-called zero point energy correction. Because the minimum of the potential energy curve is not the minimum energy of the vibrational ground state, we calculate the quantity

$$\text{ZPE}_{\text{corr}} = \epsilon_{\text{ZPE}_{\text{prod}}} - \epsilon_{\text{ZPE}_{\text{react}}} \quad (11)$$

In this way we can refer all calculated energies to the same level, thus providing better means of comparison between the energies.

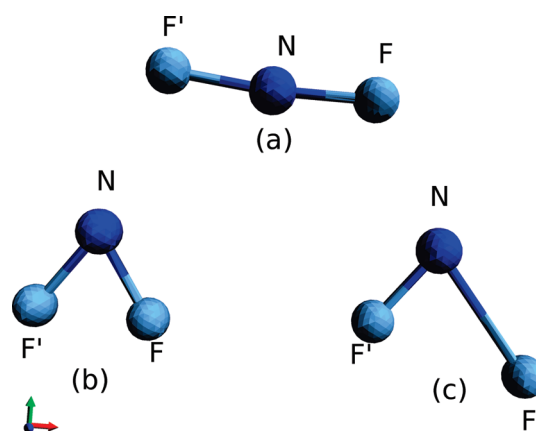
The optimized geometries and frequencies for the transition states are shown in Table 3. The optimization was carried out at the full MP2 level of theory for the cc-pVDZ and 6-31G(d) basis set. A schematic representation of the TS1 (exchange), TS2 (abstraction), and TS3 (unimolecular) transition structure geometries at MP2/cc-pVDZ level are shown in Figure 1.

It is worthy to mention the presence of the imaginary frequency, which characterizes the transition states. The zero point energy was scaled by the same factors in the three reactive systems, and it is also shown to provide a precise way to compare the obtained values.

The zero point energy correction is also important when it comes to the investigation of formation enthalpy. Zero point corrected reactant and product formation enthalpy are shown in Table 4 along with the comparison with other values in the literature. We can readily see that our values are in good agreement with both theoretical and experimental evidence.

Table 3. Transition State Geometrical Parameters (Interatomic Distances in Å and Bond Angles in Degrees), Harmonic Vibrational Frequencies (cm^{-1}), and Zero-Point Energy (kcal mol^{-1}) Calculated at MP2/cc-pVDZ and MP2/6-31G(d) Levels for the Unimolecular (TS1), Abstraction (TS2), and Exchange (TS3) Reactions; The Imaginary Frequency (ν_i) Was Also Reported

	$\text{NF}_2 = \text{NF} + \text{F}$		$\text{NF} + \text{F} = \text{N} + \text{F}_2$		$\text{NF} + \text{F} = \text{NF} + \text{F}$	
	cc-pVDZ	6-31G(d)	cc-pVDZ	6-31G(d)	cc-pVDZ	6-31G(d)
R_{NF}	1.341	1.324	1.5071	1.476	1.553	1.548
$R_{\text{NF}'}$	1.639	1.663			1.553	1.548
R_{FF}			1.520	1.580		
A_{FNF}	118.914	119.346	118.914	119.346	175.617	175.617
ν_1	311.17	288.31	633.89	626.59	651.03	669.40
ν_2	1145.52	1167.23	1046.14	1027.24	1457.81	1386.98
ν_i	806.66i	753.13i	1016.81i	843.55i	1654.30i	1601.10i
ϵ_{ZPE}	2.0364	2.0035	2.3486	2.2764	2.9481	2.8305

**Figure 1.** Schematic representation of transition structures for (a) exchange (TS1), (b) abstraction (TS2), and (c) unimolecular (TS3) reactions.

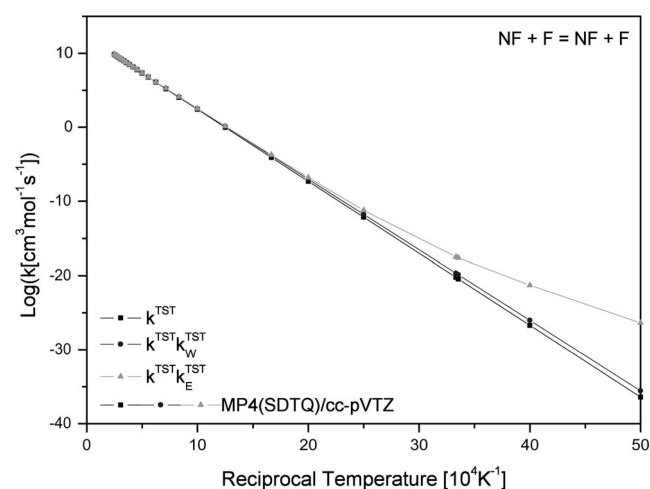
Ab initio total electronic energies, forward barrier ($V_f + \text{ZPE}_{\text{corr}}$), reverse barrier ($V_r + \text{ZPE}_{\text{corr}}$), calculated ΔH^0 at 298 K (ΔH^0 at 0 K + ZPE_{corr} and experimental ΔH^0) are shown in the Supporting Information. All these properties were calculated using all level of theory and basis sets described in section 2 for reactant, product, and TS for the exchange, abstraction, and unimolecular reactions. From these data, one can see the minor difference between ab initio and experimental ΔH^0 of exchange, abstraction, and unimolecular reactions, obtained using MP4/cc-pVTZ level. Taking that into account the final exchange, abstraction, and unimolecular TRC were calculated using MP4/cc-pVTZ level. Once we have all the energies, geometries, and frequencies for reactants, products, and transition states, we can make use of the formalism presented in section 1 to calculate TRC in the scope of the Transition State Theory.

From this point on, the section is divided into three subsection, each one dealing with a different channel of the treated system.

Exchange Channel. Figure 2 shows Conventional, Wigner, and Eckart plots of thermal rate constants against the reciprocal temperature in the range of 200–4000 K for the exchange reaction. In terms of TRC, we obtained a similar behavior of the conventional, Wigner corrected and Eckart corrected curves in

Table 4. Reactant and Product Formation Enthalpy (kcal mol^{-1}) with ZPE Correction for All Species Involved in the Unimolecular, Abstraction, and Exchange Reactions

species	this work	exp. ref.	theor. ref.
F		18.47 ± 0.07 , ¹⁹ 18.46 ± 0.07 , ²⁷ 18.92 ²⁶	
N		112.53 ± 0.02 , ¹⁹ 112.53 , ²⁷ 112.97 ± 0.1 ²⁶	
F ₂	0.403	0 ^{19,27,28}	0.3 , ^{29,30} 0.688 , ³¹ 1.288 , ³² 0.980 , ¹¹ 0.056 , ¹¹ 0.686 ¹¹
NF	53.757	55.688 ± 0.720 , ²⁷ 55.6 ± 0.5 , ³³ 59.501 ± 7.890 ¹⁹	54.9 , ²⁹ 54 , ³⁴ 53.9 , ³⁵ 56.18 , ³⁶ 46.698 , ¹¹ 54.635 , ¹¹ 51.903 ¹¹
NF ₂	7.234	10.70 ± 1.91 , ¹⁹ 8.80 ± 1.20 , ²⁷ 8 ± 1 , ²⁶ 8.3 ± 0.5 ³³	6.6 , ²⁹ 8 , ³⁴ 8.5 , ²⁹ 8.67 , ³⁶ -3.411 , ¹¹ 5.845 , ¹¹ 5.852 , ¹¹

**Figure 2.** Conventional, Wigner, and Eckart plots of thermal rate constants against the reciprocal temperature in the range of 200–4000 K for the $\text{NF} + \text{F} = \text{NF} + \text{F}$ exchange reaction.

the range 400–4000 K which is consistent to the calculated Skew angle of 54.85° , for this channel. We can note that tunneling effects are important as temperatures fall below 400 K. This is the case that Eckart corrected curve deviates from the others. The exchange reaction rate in the Arrhenius form is expressed as

$$\kappa^{\text{TST}} = 1.2293 \times 10^{11} T^{0.3238} \exp - 4413/RT$$

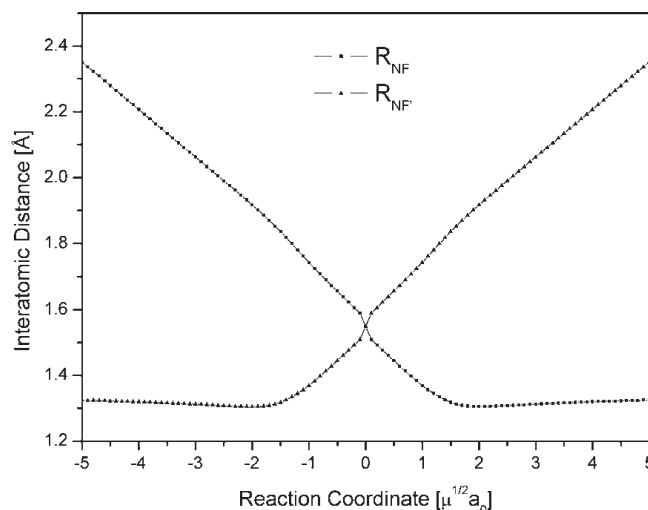
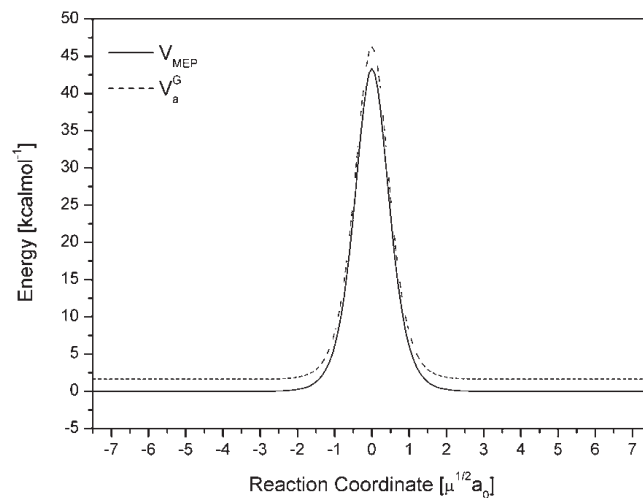
$$\kappa_W^{\text{TST}} = 4.3386 \times 10^{10} T^{0.43614} \exp - 4315/RT$$

$$\kappa_E^{\text{TST}} = 5.9521 \times 10^{-2} T^{4.197} \exp - 3240/RT$$

for the conventional (κ^{TST}), Wigner corrected (κ_W^{TST}) and Eckart corrected (κ_E^{TST}) reaction rate, respectively. It is important to note the great difference between the activation energy of conventional TST and Eckart corrected rate in the Arrhenius form. As it will be seen, this feature is presented in all channels studied and is a consequence of the fitting from the TST rate to this analytical expression.

We determined the intrinsic reaction coordinate (IRC) for the exchange channel and represented it in Figure 3 in order to understand this reaction mechanism. From this figure we can observe an increase of the NF distance with a simultaneous decrease of the NF' distance, representing the exchange between F atoms.

Figure 4 contains the V_{MEP} and V_a^G plots along the minimum energy path, as a function of reaction coordinate, for the exchange channel. This potential curve presents negligible variation from $-\infty$ to $-2 \mu^{1/2} a_0$, and then increases gradually from -2 to 0 . The curve then decreases after passing the transition

**Figure 3.** IRC for the $\text{NF} + \text{F} = \text{NF} + \text{F}$ exchange reaction.**Figure 4.** V_{MEP} and V_a^G as function of reaction coordinate for the $\text{NF} + \text{F} = \text{NF} + \text{F}$ exchange reaction.

state, presenting no global enthalpy variation, which is a well-known feature of this kind of reaction.

Abstraction Channel. The abstraction conventional, Wigner, and Eckart plots of thermal rate constants against the reciprocal temperature in the range of 200–4000 K are represented in Figure 5. We can observe a great coincidence of the conventional and corrected curves, especially for high temperature regimes. Nevertheless, for low temperatures, we can note a considerable deviation of the Eckart corrected curve, which might indicate the importance of

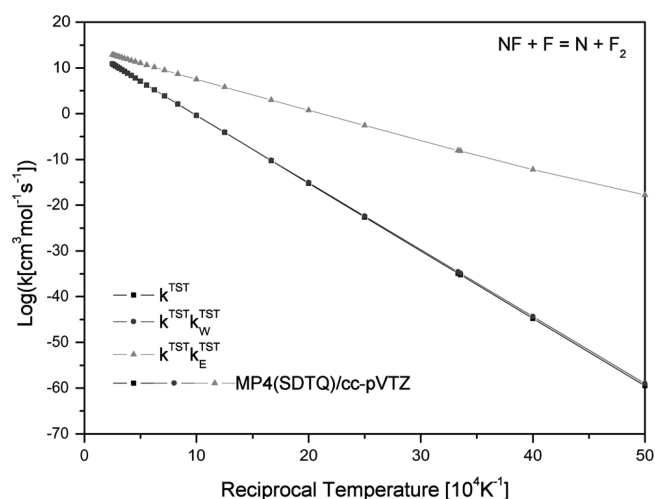


Figure 5. Conventional, Wigner, and Eckart plots of thermal rate constants against the reciprocal temperature in the range of 200–4000 K for the $\text{NF} + \text{F} = \text{N} + \text{F}_2$ abstraction reaction.

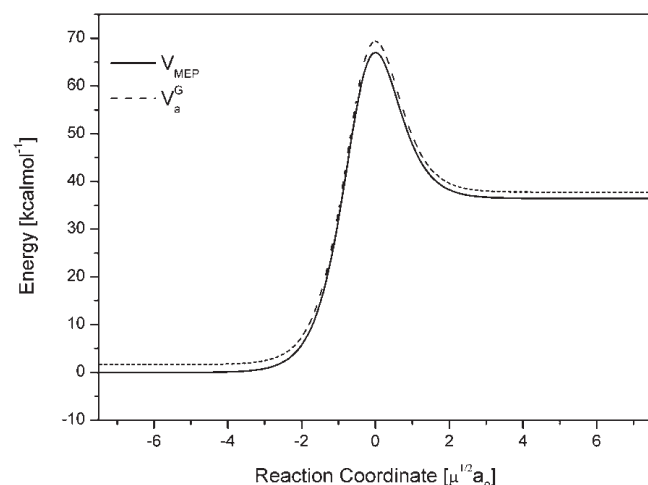


Figure 6. V_{MEP} and V_a^G as a function of reaction coordinate for the $\text{NF} + \text{F} = \text{N} + \text{F}_2$ abstraction reaction.

tunneling effects in this regime. It is important to note that this is actually of relative importance since our Skew angle for this channel resulted in the intermediate value of 62.547° and we are more interested in the high temperature regime. In this case, the Arrhenius fit for the three curves resulted in

$$\kappa^{\text{TST}} = 9.1457 \times 10^{12} T^{0.44021} \exp - 67238/RT$$

$$\kappa_{\text{W}}^{\text{TST}} = 3.2914 \times 10^{12} T^{0.55574} \exp - 66614/RT$$

$$\kappa_{\text{E}}^{\text{TST}} = 1.4233 \times 10^{10} T^{1.1991} \exp - 28718/RT$$

Figure 6 contains the V_{MEP} and V_a^G plots along the minimum energy path, as a function of reaction coordinate for this abstraction channel. The potential curve changes slowly, from $-\infty$ to $-8 \mu^{1/2} a_0$, and it increases gradually after $-8 \mu^{1/2} a_0$ and decreases quickly after passing the transition state. It characterizes an endothermic reaction.

Unimolecular Channel. Figure 7 shows the unimolecular conventional, Wigner, and Eckart plots of thermal rate constants

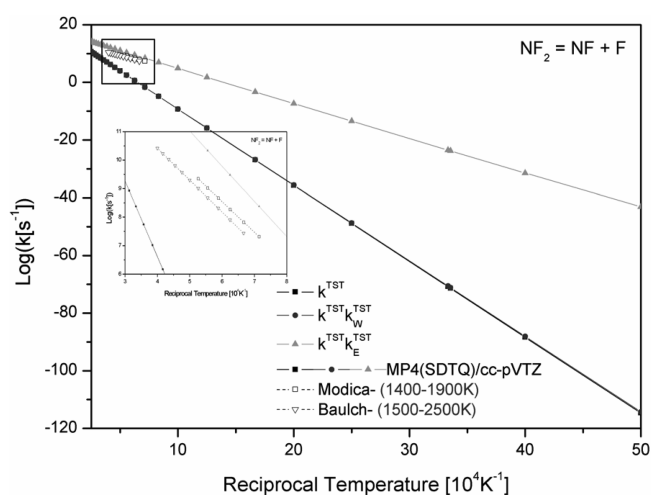


Figure 7. Conventional, Wigner, and Eckart plots of thermal rate constants against the reciprocal temperature in the range of 200–4000 K for the $\text{NF}_2 = \text{NF} + \text{F}$ unimolecular reaction.

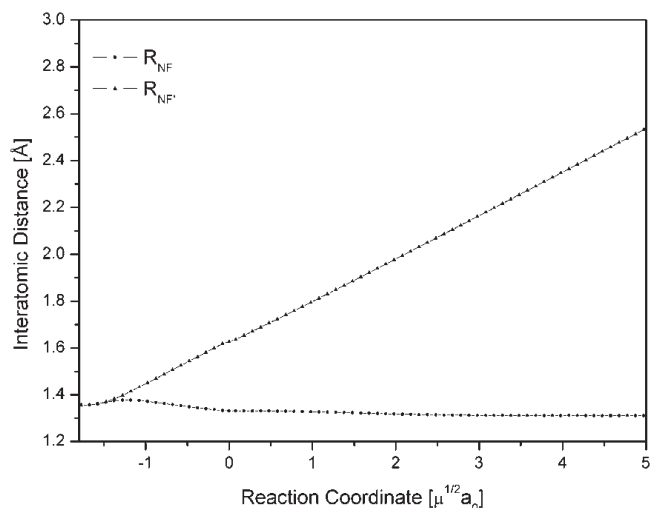


Figure 8. IRC for the $\text{NF}_2 = \text{NF} + \text{F}$ unimolecular reaction.

against the reciprocal temperature in the range of 200–4000 K. From this figure, one can note that for the temperature ranges of 1400–1900 K and 1500–2500 K the unimolecular Eckart thermal rate constants agree very well with the experimental evidence of Modica et al.¹⁷ and Baulch et al.,¹⁸ respectively. These facts allow us to trust the methodology used and the results of the preview channels. In this case, we can note that tunneling effects are of major importance even in intermediate temperature ranges. For this channel, we obtained as reaction rate

$$\kappa^{\text{TST}} = 2.027 \times 10^{16} T^{0.2430} \exp - 12045/RT$$

$$\kappa_{\text{W}}^{\text{TST}} = 8.685 \times 10^{15} T^{0.3396} \exp - 11998/RT$$

$$\kappa_{\text{E}}^{\text{TST}} = 1.3285 \times 10^{15} T^{0.56119} \exp - 54771/RT$$

The intrinsic reaction coordinate is represented in Figure 8. The monotonic distance increasing between the atoms of both NF' and NF diatoms is presented. It thus refers to the dissociation of the NF_2 molecule.

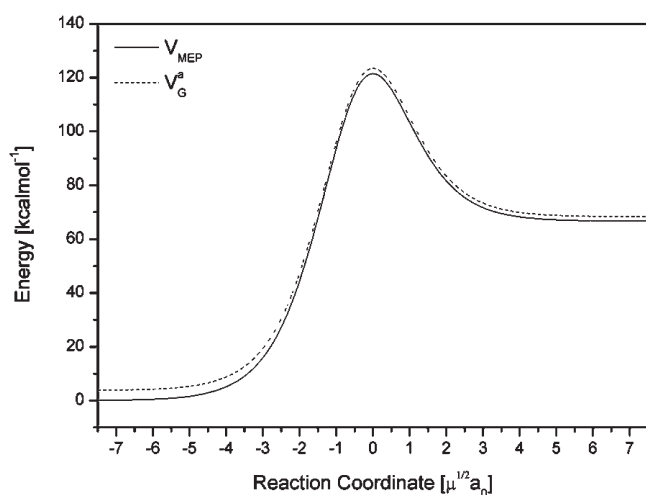


Figure 9. V_{MEP} and V_G^a as a function of reaction coordinate for the $\text{NF}_2 = \text{NF} + \text{F}$ unimolecular reaction.

The minimum energy path for the unimolecular channel is plotted in Figure 9, which, as we can see, presents the same qualitative behavior as that of the abstraction reaction previously mentioned.

CONCLUSIONS

To better understand the decomposition process of nitrogen trifluoride, we performed an accurate ab initio study in the three channels of the reactive system involving NFF, namely, $\text{NF}_2 = \text{NF} + \text{F}$, $\text{NF} + \text{F} = \text{N} + \text{F}_2$, and $\text{NF} + \text{F} = \text{NF} + \text{F}$. The best enthalpy of the unimolecular, abstraction, and exchange reactions were found at MP4/cc-pVTZ level. Through this study, we were able to obtain properties necessary to perform TST calculation and investigate reaction rate of each reaction. For the unimolecular system, we were able to obtain TRC in a good agreement with experimental data. This fact strongly suggests that the methodology used is reliable and, thus, should be applied in order to understand the important mechanism of all reactions involved in the NF_3 decomposition.

ASSOCIATED CONTENT

Supporting Information. Ab initio total electronic energies, forward barrier, reverse barrier, calculated ΔH^0 at 298 K, and experimental $\Delta_f H^0$. This material is available free of charge via the Internet at <http://pubs.acs.org>.

AUTHOR INFORMATION

Corresponding Author

*Tel.: +55(61) 3307-2900. Fax: +55(61) 3307-2363. E-mail: gargano@fis.unb.br.

ACKNOWLEDGMENT

The authors are grateful to the CENAPAD-SP for the provision of computational facilities and also to FINATEC and CNPq for financial support.

REFERENCES

- (1) Shaw, M. J.; Jones, J. D. C. *Appl. Phys.* **1977**, *14*, 393.

- (2) Antoniotti, P.; Grandinetti, F. *Chem. Phys. Lett.* **2002**, *366*, 676.
- (3) Donnelly, V. M.; Flamm, D. L.; Dautremont-Smith, W. C.; Werder, D. J. *J. Appl. Phys.* **1984**, *55*, 242.
- (4) Wang, J. J.; Lambers, E. S.; Pearton, S. J.; Ostling, M.; Zetterling, C. M.; Grow, J. M.; Ren, F. *Solid-State Electron.* **1998**, *42*, 743.
- (5) Ramalho, S. S.; Barreto, P. R. P.; Martins, J. B. L.; e Silva, G. M.; Gargano, R. J. *Phys. Chem. A* **2009**, *113*, 14336.
- (6) Truhlar, D. G.; Isaacson, A. D.; Garrett, B. C. *Theory of Chemical Reaction Dynamics*; CRC Press, Inc., Oxford Science: Boca Raton, FL, 1985; Vol. 2.
- (7) Eckart, C. *Phys. Rev.* **1930**, *35*, 1303.
- (8) Frisch, M. J.; Trucks, G. W.; Schlegel, H. B.; Scuseria, G. E.; Robb, M. A.; Cheeseman, J. R.; Montgomery, J. A., Jr.; Vreven, T.; Kudin, K. N.; Burant, J. C.; Millam, J. M.; Iyengar, S. S.; Tomasi, J.; Barone, V.; Mennucci, B.; Cossi, M.; Scalmani, G.; Rega, N.; Petersson, G. A.; Nakatsuji, H.; Hada, M.; Ehara, M.; Toyota, K.; Fukuda, R.; Hasegawa, J.; Ishida, M.; Nakajima, T.; Honda, Y.; Kitao, O.; Nakai, H.; Klene, M.; Li, X.; Knox, J. E.; Hratchian, H. P.; Cross, J. B.; Bakken, V.; Adamo, C.; Jaramillo, J.; Gomperts, R.; Stratmann, R. E.; Yazyev, O.; Austin, A. J.; Cammi, R.; Pomelli, C.; Ochterski, J. W.; Ayala, P. Y.; Morokuma, K.; Voth, G. A.; Salvador, P.; Dannenberg, J. J.; Zakrzewski, V. G.; Dapprich, S.; Daniels, A. D.; Strain, M. C.; Farkas, O.; Malick, D. K.; Rabuck, A. D.; Raghavachari, K.; Foresman, J. B.; Ortiz, J. V.; Cui, Q.; Baboul, A. G.; Clifford, S.; Cioslowski, J.; Stefanov, B. B.; Liu, G.; Liashenko, A.; Piskorz, P.; Komaromi, I.; Martin, R. L.; Fox, D. J.; Keith, T.; Al-Laham, M. A.; Peng, C. Y.; Nanayakkara, A.; Challacombe, M.; Gill, P. M. W.; Johnson, B.; Chen, W.; Wong, M. W.; Gonzalez, C.; Pople, J. A. *Gaussian 03*, Revision D.01, Gaussian, Inc.: Wallingford, CT, 2004.
- (9) Pilling, M. J.; Seakins, P. W. *Reaction Kinetic*, Vol. 4. Oxford Science, Oxford, UK, second ed., 1995.
- (10) Barreto, P. R. P.; Vilela, A. F. A.; Gargano, R. J. *Mol. Struct. (THEOCHEM)* **2003**, *639*, 167.
- (11) Barreto, P. R. P.; Vilela, A. F. A.; Gargano, R. *Int. J. Quantum Chem.* **2005**, *103*, 685.
- (12) Ramalho, S. S.; Barreto, P. R. P.; Vilela, A. F. A.; Gargano, R. *Chem. Phys. Lett.* **2005**, *413*, 151.
- (13) Truong, T. N.; Truhlar, D. G. *J. Chem. Phys.* **1990**, *93*, 1761.
- (14) Pardo, L.; Banfelder, J. R.; Osman, R. *J. Am. Chem. Soc.* **1992**, *114*, 2382.
- (15) Henon, E.; Bohr, F. J. *Mol. Struct. (THEOCHEM)* **2000**, *531*, 283.
- (16) Johnston, H. S.; Heicklen, J. J. *Phys. Chem.* **1962**, *66*, 532.
- (17) Modica, A. P.; Hornig, D. F. *J. Chem. Phys.* **1965**, *43*, 8.
- (18) Baulch, D. L.; Grant, S. J.; Montague, D. C. *J. Phys. Chem. Ref. Data (Suppl.)* **1981**, *10* (1).
- (19) Chase, M. W. J. *Phys. Chem. Ref. Data* **1998**.
- (20) Radzig, A. A.; Smirnov, B. M. *Reference Data on Atoms, Molecules and Ions*; Springer-Verlag: Berlin, 1985.
- (21) Herzberg, G. *Molecular Spectra and Molecular Structure I. Spectra of Diatomic Molecules*, 2nd ed.; Van Nostrand Reinhold Company: New York, 1950; Vol. 1.
- (22) Barreto, P. R. P.; Vilela, A. F. A.; Gargano, R. *Int. J. Quantum Chem.* **2005**, *103*, 659.
- (23) Bettendorff, M.; Peyerimhoff, S. D. *Chem. Phys.* **1985**, *99*, 55.
- (24) Chase, M. W. J. *Phys. Chem. Ref. Data Monog.* **1998**, *9*.
- (25) Harmony, M. D.; Myers, R. J. *J. Chem. Phys.* **1962**, *37*, 636.
- (26) West, R. C.; Astle, M. J.; Beyer, W. H., Eds. *CRC Handbook of Chemistry and Physics*; CRC Press: Boca Raton, FL, 1985.
- (27) Gurvich, L. V.; Veyts, I. V.; Alcock, C. B. *Thermodynamic Properties of Individual Substances*, 4th ed.; Hemisphere Pub. Co.: New York, 1989.
- (28) Benson, S. W. *Thermochemical Kinetics - Methods for the Estimation of Thermochemical Data and Rate Parameters*; John Wiley and Sons: New York, 1960.
- (29) Berkowitz, J.; Greene, J. P.; Foropoulos, J., Jr.; Neskovic, O. M. *J. Phys. Chem. A* **2001**, *105*, 8533.
- (30) Curtiss, L. A.; Raghavachari, K.; Redfern, P. C.; Rassolov, V.; Pople, J. A. *J. Chem. Phys.* **1997**, *106*, 1063.

- (31) Curtiss, L. A.; Raghavachari, K.; Redfern, P. C.; Rassolov, V.; Pople, J. A. *J. Chem. Phys.* **1998**, *109*, 7764.
- (32) Curtiss, L. A.; Raghavachari, K.; Redfern, P. C.; Rassolov, V.; Pople, J. A. *J. Chem. Phys.* **1999**, *110*, 4703.
- (33) Berkowitz, J.; Greene, J. P.; Foropoulos, J., Jr.; Neskovic, O. M. *J. Chem. Phys.* **1984**, *81*, 6166.
- (34) Aschi, M.; Grandinetti, F. *J. Mol. Struct. (THEOCHEM)* **2000**, *497*, 205.
- (35) Melius, C. F.; Ho, P. *J. Phys. Chem.* **1998**, *95*, 1410.
- (36) Ricca, A. *Chem. Phys. Lett.* **1998**, *294*, 454.